PHYSICAL REVIEW C VOLUME 23, NUMBER 6 JUNE 1981

Relativistic heavy ions measure the momentum distribution on the nuclear surface

J. Hüfner and M. C. Nemes
Institut für Theoretische Physik der Universität and Max-Planck-Institut für Kernphysik, D-6900 Heidelberg, Federal Republic of Germany
(Received 29 December 1980)

In fragmentation reactions of the type ^{16}O + target$\rightarrow{}^{15}O + X$, the momentum distribution of the outgoing fragment ^{15}O reflects the momentum distribution of the nucleon which is removed from the surface of the projectile nucleus. We derive a relation using Glauber's multiple scattering theory and the Wigner transform of the one-body density matrix. The experimental cross section at 2 GeV/nucl is analyzed with the following result: The uniform and local Fermi-gas models fail to reproduce the momentum distribution on the surface. The shell model with harmonic oscillator wave functions is correct for momenta below the Fermi momentum. Hartree-Fock wave functions describe the data up to 350 MeV/c.

[NUCLEAR REACTIONS Heavy ions, relativistic energies; fragmentation reactions; relation to nuclear momentum distribution on the surface.]

I. INTRODUCTION

How is matter distributed in the nucleus? Various experiments with electrons, mesons, protons, and α particles have resulted in a consistent and very detailed picture of nuclear charge and matter densities. How is motion distributed in the nucleus? Do nucleons move faster in the center and slower on the surface? We still lack detailed quantitative information. Quasielastic electron scattering experiments[1] measure the global mean square momentum $\langle\vec{k}^2\rangle$ or equivalently the Fermi momentum $p_F = (5\langle\vec{k}^2\rangle/3)^{1/2}$ of the protons. Experiments[2] of the type $(e, e'p)$ map the single-particle wave function of the knocked-out nucleon but not for the large momentum components. In particular, how is momentum distributed in the nuclear surface? Experiments with relativistic heavy ions may answer this question. The present paper relates quantitatively the momentum distribution observed in fragmentation reactions to the momentum distribution on the nuclear surface.

In reactions of the type

$$^{16}O + \text{target} \rightarrow {}^{15}O + X \ , \tag{1.1}$$

the momentum of the outgoing fragment ^{15}O is measured, while everything else remains unobserved. If $\vec{k}$ denotes the momentum of the final fragment in the rest system of the projectile, an inclusive cross section $d^3\sigma/d\vec{k}^3$ can be measured. The momentum vector $\vec{k} = (\vec{k}_\perp, k_\parallel)$ is usually decomposed into a component $k_\parallel$, parallel to the beam, and the transverse part $\vec{k}_\perp$. Situations with $k_\parallel > 0$ are particularly interesting. The fragment is faster than the projectile. Since the stripping of a nucleon cannot accelerate the projectile, the extra forward momentum must have been present in the projectile before the collision. This hypothesis is supported by the fact that experimental shapes of $d^3\sigma/d\vec{k}^3$ do not depend on energy nor on the target.[3] Goldhaber[4] has been the first to relate the width of $d^3\sigma/d\vec{k}^3$ to the nuclear Fermi momentum. Abul-Magd *et al.*[5] and Fujita *et al.*[6] have followed up this idea. Fragmentation reactions at much lower energies (40 MeV/nucleon) have been analyzed in a similar spirit (Shyam *et al.*[7]). However, the quantitative relation between cross sections and momentum distributions is not yet sufficiently clear in the sense that reaction dynamics and nuclear structure are not clearly separated. This also holds true for the earlier attempts to describe high energy deuteron breakup in the field of the nucleus by Glauber,[8] Akhiezer *et al.*,[9] Bertocchi *et al.*,[10] and Kühn *et al.*[11]

In this paper we try to give a transparent and quantitative relation between $d^3\sigma/d\vec{k}^3$ and the momentum distribution on the nuclear surface. The following physical picture underlies the calculation: Since the fragment ^{15}O in Eq. (1.1) has to survive in a bound state, the reaction proceeds peripherally. The extra neutron is removed from the nuclear surface and the ^{15}O reflects its momentum distribution. Can there be *momentum* distribution on the nuclear *surface*? Does the uncertainty principle allow us to define a momentum distribution in a localized region of space? The appropriate tool to handle this problem correctly is the Wigner transform W of the one-body density matrix $\langle\vec{r}|\,\rho\,|\vec{r}'\rangle$

$$W(\vec{R};\vec{p}) = \int \frac{d^3x}{(2\pi)^3}\, e^{-\vec{p}\cdot\vec{x}} \left\langle \vec{R} - \frac{\vec{x}}{2} \middle|\, \rho \,\middle| \vec{R} + \frac{\vec{x}}{2} \right\rangle . \tag{1.2}$$

This quantity represents the "probability" of finding a particle with momentum $\vec{p}$ at position $\vec{R}$. We write probability in quotation marks because W need not be positive. Only certain integrals of W are. In this paper we derive the following relation between W and the fragmentation cross section $d^3\sigma/dk^3$

$$\frac{d\sigma}{dk_\parallel} \equiv \int d^2k_\perp \frac{d^3\sigma}{dk^3} = \int d^2s\, D(\vec{s}) \int dz \int d^2k_\perp W(\vec{s}, z; \vec{k}_\perp, k_\parallel - \langle k_\parallel \rangle) . \tag{1.3}$$

The distorting function $D(\vec{s})$ contains the reaction dynamics and localizes the reaction to the nuclear surface. The Wigner transform W contains the momentum distribution of the removed nucleon. The derivation of Eq. (1.3) from Glauber theory as well as its conditions of validity are the subject of the next section. Then, in Sec. III, the experimental data are compared with several models for the nuclear momentum distribution. In particular, Fermi gas models are ruled out. The paper closes with a discussion of desirable further experiments.

II. DERIVATION OF THE CROSS SECTION

The cross section for a fragmentation reaction of the type of Eq. (1.1) is calculated from Glauber's multiple scattering formalism.[12] The notation is summarized in the following equation, valid in the projectile's rest system:

$$^AZ\{|\vec{0}, \Psi_0\rangle\} + \text{target}\{|-\vec{P}_0, \Theta_0\rangle\} \to {}^{A-1}Z\{|\vec{k}, \Phi_\alpha\rangle\} + n\{|\vec{p}, \eta_{\vec{p}}\rangle\} + (\text{target})'\{|-\vec{P}_0 - \vec{q}, \Theta_\beta\rangle\} . \tag{2.1}$$

Before the reaction, the projectile nucleus ^AZ with intrinsic wave function Ψ_0 is at rest and the target approached with momentum $-\vec{P}_0$. After the interaction a fragment with $A-1$ nucleons is detected in a particle-stable Φ_α with momentum $\vec{k}$. The neutron with momentum $\vec{p}$ and scattering wave function $\eta_{\vec{p}}$, and the final state Θ_β of the target, are unobserved. The cross section corresponding to Eq. (2.1) is given by (cf., Fujita *et al.*[6])

$$\frac{d^3\sigma}{dk^3} = \int d^2q \sum_\alpha{}' \sum_\beta \left| \int \frac{d^2b}{2\pi} e^{-i\vec{q}\cdot\vec{b}} \left\langle \eta_{\vec{q}-\vec{k}} \Phi_\alpha; \Theta_\beta \left| 1 - \prod_{\substack{i\in P \\ j\in T}} (1 - \Gamma_{ij}) \right| \Psi_0; \Theta_0 \right\rangle \right|^2 . \tag{2.2}$$

Here the $\Gamma_{ij}(\vec{x}_i + \vec{b} - \vec{y}_j)$ are the profile functions for collisions between a projectile nucleon i located at $\vec{x}_i$ and a target nucleon j at $\vec{y}_j$. $\vec{x}_i$ and $\vec{y}_j$ refer to the respective centers of mass and the impact parameter $\vec{b}$ is the transverse distance between projectile and target. As usual in Glauber theory, energy conservation is neglected. This approximation is good except close to the kinematical limit in k (cf., Fig. 3 of Ref. 6). If E_0 is the total laboratory energy of the projectile and M_0 its mass, then the maximal forward momentum $k_\parallel^{\max}$ of the fragment in the projectile rest system given by

$$k_\parallel^{\max} = \frac{E_0}{M_0}(E_0 - m)\left\{\left[1 - \left(\frac{M_0 - m}{E_0 - m}\right)^2\right]^{1/2} - \left[1 - \left(\frac{M_0}{E_0}\right)^2\right]^{1/2}\right\} \xrightarrow[E_0 \to \infty]{} m\left(1 - \frac{1}{2M_0}\right), \tag{2.3}$$

where m is the nucleon mass. In Eq. (2.2) the sum over target states Θ_β is performed by closure and the sum over fragment states Φ_α is restricted to the particle-stable states (indicated by the prime on the sum). We expand the projectile's ground state into the Φ_α (neglecting antisymmetrization)

$$\Psi_0(\vec{x}_1, \ldots \vec{x}_{A_p}) = \sum_\alpha a_\alpha \varphi_\alpha(\vec{x}_1) \Phi_\alpha(\vec{x}_2, \ldots \vec{x}_{A_p}), \tag{2.4}$$

where the a_α are the spectroscopic amplitudes. During the fragmentation reaction a nucleon is lifted from a bound orbit φ_α to the scattering state $\eta_{\vec{p}}$. The two wave functions are therefore orthogonal:

$$\langle \eta_{\vec{p}} | \varphi_\alpha \rangle = 0 . \tag{2.5}$$

This relation has important consequences. With this notation the cross section Eq. (2.2) is written as

$$\frac{d^3\sigma}{dk^3} = \int d^2q \int \frac{d^2b\, d^2b'}{(2\pi)^2} e^{-i\vec{q}(\vec{b}-\vec{b}')} \sum_\alpha{}' |a_\alpha|^2 \int d^3x\, \eta^*_{\vec{q}-\vec{k}}(\vec{x}) \varphi_\alpha(\vec{x}) \int d^3x' \eta_{\vec{q}-\vec{k}}(\vec{x}') \varphi^*_\alpha(\vec{x}') G_\alpha(\vec{b}, \vec{b}', \vec{b}+\vec{s}, \vec{b}'+\vec{s}'; \lambda), \tag{2.6}$$

where $\vec{x} = (\vec{s}, z)$ and $\vec{x}' = (\vec{s}', z')$. The function G is defined by

$$G_\alpha = \int \prod_{i>1} d^3x_i \prod_{i>1} d^3x_i' \prod_j d^3y_j \, |\Theta_0(\vec{y}_1,\ldots)|^2 |\Phi_\alpha(\vec{x}_2,\ldots)|^2 |\Phi_\alpha(\vec{x}_2',\ldots)|^2 \prod_{\substack{m\in P \\ n\in T}} [1-\lambda(\Gamma_{mn}+\Gamma_{mn}^*-\Gamma_{mn}\Gamma_{mn}^*)]. \quad (2.7)$$

The profile functions Γ_{mn} depend on $(\vec{s}_m+\vec{b}-\vec{t}_n)$ and the Γ^* on $(\vec{s}_m'+\vec{b}'-\vec{t}_n')$, where $\vec{t}_n$ is the transverse component of $\vec{y}_n$. We have assumed that the fragment state Φ_α in Eq. (2.4) does not change during the collision, i.e., that elastic fragment-target collisions dominate the cross section. The parameter λ in Eq. (2.7) is introduced to define a cumulant expansion:

$$\ln G_\alpha(\lambda) = \left[\ln G_\alpha(0) + \lambda \frac{\partial G_\alpha}{\partial \lambda} G_\alpha^{-1}(0) + \cdots\right]_{\lambda=1}. \quad (2.8)$$

We truncate after the first order in λ, thus neglecting nucleon-nucleon correlations (cf., Glauber[12]). $G_\alpha(0) = 1$ and

$$\frac{\partial}{\partial\lambda} G_\alpha(\vec{b},\vec{b}';\vec{s}+\vec{b},\vec{s}'+\vec{b}';\lambda)|_{\lambda=0}$$
$$= i[\chi_{FT}(\vec{b}) - \chi_{FT}^*(\vec{b}')] + i[\chi_T(\vec{b}+\vec{s}) - \chi_T^*(\vec{b}'+\vec{s}')] + \sigma_{NN}(\vec{b}+\vec{s}-\vec{b}'-\vec{s}')\, T_T\left(\frac{\vec{b}+\vec{s}+\vec{b}'+\vec{s}'}{2}\right), \quad (2.9)$$

where χ_{FT} is the optical phase shift function for elastic fragment-target collisions

$$i\chi_{FT}(\vec{b}) \approx -\left\langle \Phi_\alpha\Theta_0 \middle| \sum_{\substack{m>1 \\ n}} \Gamma_{mn} \middle| \Phi_\alpha\Theta_0 \right\rangle. \quad (2.10)$$

Terms of the type $\Gamma_{mn}\Gamma_{mn}^*$ with $m>1$ have been dropped in (2.10) since they are small. The presumably weak dependence of the optical phase shift function on the fragment state (labeled α) will be neglected. The optical phase shift function χ_T describes elastic scattering of the removed nucleon by the target

$$i\chi_T(\vec{b}+\vec{s}) = -\left\langle \Theta_0 \middle| \sum_n \Gamma_{1n}(\vec{b}+\vec{s}-\vec{t}_n) \middle| \Theta_0 \right\rangle. \quad (2.11)$$

The inelastic interaction of the knocked-out nucleon with the target is contained in the last term of Eq. (2.9). It is proportional to the thickness function of the target

$$T_T(\vec{B}) = A_T \int dz\, \rho(\vec{B},z) \quad (2.12)$$

and to the Fourier transform of the nucleon-nucleon cross section

$$\sigma_{NN}(\vec{b}) = \int d^2q\, e^{i\vec{q}\cdot\vec{b}} \frac{d\sigma_{NN}}{d^2q}. \quad (2.13)$$

The function $\sigma_{NN}(\vec{b})$ is of short range (order 1 fm) and therefore introduces high Fourier components in the integrals of Eq. (2.6).

The reaction dynamics which are contained in G can be separated according to the magnitude of the Fourier components which are generated. The phase shift functions depend smoothly on the argument (variations over distances of the nuclear radii), while the σ_{NN} fall off rapidly. Therefore

$$G = G_{\text{coh}} + G_{\text{inc}} \quad (2.14)$$

with the "coherent part" (small Fourier components)

$$G_{\text{coh}} = \exp[i\chi_{FT}(\vec{b}) - i\chi_{FT}^*(\vec{b}') + i\chi_T(\vec{b}+\vec{s}) - i\chi_T^*(\vec{b}'+\vec{s}')] \quad (2.15)$$

and the incoherent term G_{inc}. Equation (2.15) describes those fragmentation processes in which the target remains in its ground state. Therefore, the coherent part of the cross section defined by introducing into Eq. (2.6) can be written as

$$\frac{d^3\sigma_{\text{coh}}}{dk^3} = \sum_\alpha{}' |a_\alpha|^2 \int d^2q \left| \int \frac{d^2b}{2\pi} e^{-i\vec{q}\cdot\vec{b}} e^{i\chi_{FT}(\vec{b})} \int dz\, d^2s\, \eta_{\vec{q}-\vec{k}}^*(\vec{s},z) e^{i\chi_T(\vec{b}+\vec{s})} \varphi_\alpha(\vec{s},z) \right|^2. \quad (2.16)$$

This cross section corresponds to the diffractive dissociation of the deuteron-nucleus collisions extensively discussed in Refs. 8–11. Since χ_T is a smooth function of $\vec{s}$, the orthogonality, Eq. (2.5), between η and φ_α is very important and is responsible for the smallness of the coherent contribution. For reaction (1.1) with ^{12}C as a target, the integrated coherent cross section is calculated to be of the order of 10% of the total fragmentation cross section. For this reason we neglect it in the comparison with experiment and relegate a further discussion of Eq. (2.16) to Appendix A.

The fragmentation cross section which corresponds to the incoherent processes contained in G_{inc} is written as

$$\frac{d^3\sigma}{dk^3} = \int d^2q \int \frac{d^2b\, d^2b'}{(2\pi)^2} e^{-i\vec{q}(\vec{b}-\vec{b}')} e^{i[\chi_{FT}(\vec{b})-\chi^*_{FT}(\vec{b}')]} \times \sum_\alpha |a_\alpha|^2 \int d^3x\, d^3x' \eta^*_{\vec{q}-\vec{k}}(\vec{x}) \eta_{\vec{q}-\vec{k}}(\vec{x}') \varphi_\alpha(\vec{x}) \varphi^*_\alpha(\vec{x}') \times \left(e^{i[\chi_T(\vec{b}+\vec{s})-\chi^*_T(\vec{b}'+\vec{s}')]} \left\{ \exp\left[\sigma_{NN}(\vec{b}+\vec{s}-\vec{b}'-\vec{s}') T_T\left(\frac{\vec{b}+\vec{s}+\vec{b}'+\vec{s}'}{2} \right) \right] - 1 \right\} \right) . \tag{2.17}$$

It sums all contributions in which the target is excited; see, for instance, the similarity of the operator in curly brackets to the one by Glauber and Matthiae.[13] Since the inelastic collisions by the free space NN cross sections σ_{NN} generate momentum components of the order of 0.4 GeV/c, the scattering function $\eta_{\vec{q}-\vec{k}}$ may be replaced by a plane wave (cf., also Appendix B). Then the integration over $\vec{q}$ in Eq. (2.17) leads to a δ function

$$\frac{d^3\sigma}{dk^3} = \int d^2b\, d^2b' \delta^{(2)}(\vec{b}+\vec{s}-\vec{b}'-\vec{s}') e^{i[\chi_{FT}(\vec{b})-\chi^*_{FT}(\vec{b}')]} \times \sum_\alpha{}' |a_\alpha|^2 \{ e^{\sigma_{NN}(0) T_T(\vec{b}+\vec{s})} - 1 \} \int \frac{d^3x\, d^3x'}{(2\pi)^3} e^{i\vec{k}(\vec{x}-\vec{x}')} \varphi_\alpha(\vec{x}) \varphi^*_\alpha(\vec{x}') e^{-2\,\mathrm{Im}\chi_T(\vec{b}+\vec{s})} . \tag{2.18}$$

A particularly clean result is obtained if one calculates the momentum distribution integrated over $\vec{k}_\perp$, namely

$$\frac{d\sigma}{dk_\parallel} \equiv \int dk_\perp \frac{d^3\sigma}{dk^3} . \tag{2.19}$$

The integration over $\vec{k}_\perp$ yields a $\delta^{(2)}(\vec{s}-\vec{s}')$ in Eq. (2.18) and

$$\frac{d\sigma}{dk_\parallel} = \int d^2s \left\{ \int d^2b\, e^{-2\,\mathrm{Im}\chi_{FT}(\vec{b})} [e^{-2\,\mathrm{Im}\chi_T(\vec{b}+\vec{s})} (e^{\sigma_{NN}(0) T_T(\vec{b}+\vec{s})} - 1)] \right\} \int dz\, d^2k_\perp W(\vec{s}, z; \vec{k}_\perp, k_\parallel) . \tag{2.20}$$

Here W is the Wigner transform for the removed particle

$$W(\vec{R},\vec{k}) = \int \frac{d^3r}{(2\pi)^3} e^{-i\vec{k}\vec{r}} \sum_\alpha{}' |a_\alpha|^2 \varphi^*_\alpha\left(\vec{R}-\frac{\vec{r}}{2}\right) \varphi_\alpha\left(\vec{R}+\frac{\vec{r}}{2}\right) . \tag{2.21}$$

Equation (2.20) is the form of Eq. (1.3) except for the small shift $\langle k_\parallel \rangle$ discussed in Appendix B. The nuclear structure information, i.e., the momentum distribution in the projectile ground state, is contained in the Wigner transform while the term in curly brackets describes the reaction mechanism and may be written as a function $D(s)$. The phase shift function χ_{FT} ensures that target and fragment are kept a distance $|\vec{b}| \geq R_F + R_T$ apart. The term in the square bracket is maximum for $|\vec{b}+\vec{s}| \approx R_T$, where the knock-out takes place. The Wigner transform vanishes for $|\vec{s}| \gtrsim R_P$. For these reasons the expression is largest on the projectile's surface $|\vec{s}| \approx R_P$. Details are postponed to the next section.

While the Wigner transform need not be positive definite, the expression appearing in Eq. (2.20) must be because the cross section is positive. This is a consequence of the following particular situation: $k_\parallel$ is observed and z is integrated over (thus washing out any spatial information in z direction). Conversely, the transverse spatial components are localized to the surface by the reaction dynamics, but $\vec{k}_\perp$ is integrated over. For these reasons there are no problems with the uncertainty relation.

In the actual experiment[3] the quantity in Eq. (2.20) is not measured but rather $d^3\sigma/dk^3$ for $\vec{k}_\perp = 0$ and also for $k_\parallel = 0$. The corresponding theoretical expression is only obtained after a further approximation: Since the reaction is localized in impact parameter and $\vec{b}-\vec{b}'$ is small, one can expand

$$i[\chi_{FT}(\vec{b}) - \chi^*_{FT}(\vec{b}')] \approx -2\,\mathrm{Im}\chi_{FT}\left(\frac{\vec{b}+\vec{b}'}{2}\right) + i(\vec{b}-\vec{b}') \cdot \nabla\, \mathrm{Re}\chi_{FT}\left(\frac{\vec{b}+\vec{b}'}{2}\right) . \tag{2.22}$$

Then

$$\frac{d^3\sigma}{dk^3} \approx \int d^2s \int d^2b\, e^{-2\,\mathrm{Im}\chi_{FT}(\vec{b})} e^{-2\,\mathrm{Im}\chi_T(\vec{b}+\vec{s})} [e^{\sigma_{NN}(0) T_T(\vec{b}+\vec{s})} - 1] \int dz\, W[\vec{s}, z; \vec{k} - \mathrm{Re}\nabla\chi_{FT}(\vec{b})] . \tag{2.23}$$

The additional transverse momentum $\Delta\vec{k}_\perp = -\mathrm{Re}\vec{\nabla}\chi_{FT}$ which appears in the argument of Eq. (2.23) is acquired by the fragment when it scatters elastically from the target. Thus according to Eq. (2.23) the momentum distribution $d^3\sigma/dk^3$ is not directly related to the momentum distribution in the target. Difficulties are particularly evident in transverse direction. This has been observed already in Refs. 6 and 11. Furthermore, the integration over $\vec{b}$ is more complicated and reaction dynamics and nuclear structure are no more so clearly separated as in Eqs. (1.3) and (2.20).

III. CALCULATION AND COMPARISON WITH EXPERIMENT

As derived in the previous section, the fragmentation cross section $d\sigma/dk_\parallel$, Eq. (2.20), reflects the momentum distribution on the nuclear surface in a way which needs the least number of assumptions. Unfortunately, $d\sigma/dk_\parallel$ is not measured[3] but rather the cross section $(d^3\sigma/dk^3)_{k_\perp=0}$. For the comparison with experiment we shall use the expression

$$\left(\frac{d^3\sigma}{dk^3}\right)_{\vec{k}_\perp=0} = \int d^2s\, D(s) \times \int dz\, W(\vec{s},z;k_\parallel - \langle k_\parallel\rangle, \vec{k}_\perp = 0)\,, \tag{3.1}$$

with the Wigner transform W from Eq. (2.21) and the distorting function

$$D(s) = \int d^2b\, e^{-2\,\mathrm{Im}\chi_{FT}(\vec{b}) - 2\,\mathrm{Im}\chi_T(\vec{b}+\vec{s})} \times \left[e^{\sigma_{NN}T_T(\vec{b}+\vec{s})} - 1\right]. \tag{3.2}$$

The symbols are explained in the previous section. The expression (3.1) is derived from the Glauber theory with the additional assumption that the momentum transfer $\Delta k_\perp = -\mathrm{Re}\nabla\chi_{FT}$ can be neglected. This momentum arises from elastic fragment-target scattering. The neglect seems justified for the high energy reaction under consideration for the following two reasons:

(i) This momentum transfer is *transverse*, but we are interested only in the *longitudinal* dependence $k_\parallel$. For a pure Gaussian wave function the longitudinal and transverse momentum directions in the Wigner transform are completely decoupled. For ^{16}O with its $1p$ orbits this still holds to a good approximation.

(ii) The additional momentum $\Delta k_\perp$ is estimated to be of the order of several tens of MeV/c and therefore small compared to the mean transverse momentum of about 100 MeV/c for the experimental distribution.

In this paper we investigate the reaction

$$^{16}\mathrm{O} + {}^{12}\mathrm{C} \rightarrow {}^{15}\mathrm{O} + X \tag{3.3}$$

at 2.1 GeV/nucleon. The data are taken from Greiner *et al.*[3] The experimental distribution in $k_\parallel$ covers the range $|k_\parallel| < 350$ MeV/c for $k_\perp = 0$. The kinematical limit Eq. (2.1) for 2.1 GeV/nucleon ^{16}O projectiles is $k_\parallel^{\max} = 640$ MeV/c and large compared to the observed $k_\parallel$. Therefore, energy conservation can be safely neglected. The choice of a light target in reaction (3.3) is advocated since the coherent breakup of the projectile due to the Coulomb interaction with the target is small. We extrapolate the analysis by Heckman *et al.*[14] to ^{12}C as target and estimate 1 mb for the contribution of Coulomb dissociation to reaction (3.3). Similarly, the coherent breakup of ^{16}O due to elastic scattering by ^{12}C is small and estimated to be below 5 mb (Appendix A).

Two functions enter the calculation of the cross section, Eq. (3.1): the distortion function $D(s)$, which contains all the reaction dynamics, and the Wigner transform W, which reflects nuclear structure. The distortion function is calculated with no free parameters. Realistic densities for the matter distribution of the projectile are used, a Gaussian density for the target is used, and $\sigma_{NN} = 40$ mb.

We calculate the integrated fragmentation cross section

$$\sigma_F = \int d^3k\, \frac{d^3\sigma}{dk^3} = \int ds\, \frac{d\sigma}{ds}. \tag{3.4}$$

The integrand in Eq. (3.4) represents the probability for the abrasion of one nucleon as a function of its distance from the center. Explicitly,

$$\frac{d\sigma}{ds} = 2\pi s\, D(s)\, T_P(s), \tag{3.5}$$

where T_P is the thickness function for the nucleon which is removed from the projectile. $d\sigma/ds$ is displayed in Fig. 1 and it is clearly most important for values of s which are larger than the rms radius of ^{16}O, i.e., at positions where the nuclear matter is thin. Figure 1 substantiates our claim that the nucleon is abraded from the nuclear surface (removal of a $1s$ nucleon is unlikely since it is more localized in the interior). Using Eq. (3.4) and applying the reduction factor of about $\frac{1}{2}$ due to final state interaction (Appendix B), we find

$$\sigma_F^{\mathrm{calc}} = 57 \text{ mb},$$
$$[\sigma_F^{\mathrm{exp}} = (42 \pm 2) \text{ mb}] \text{ (see Ref. 15).} \tag{3.6}$$

We discuss the shape of the fragmentation cross section $(d^3\sigma/dk^3)_{k_\perp=0}$. It reflects directly the mo-

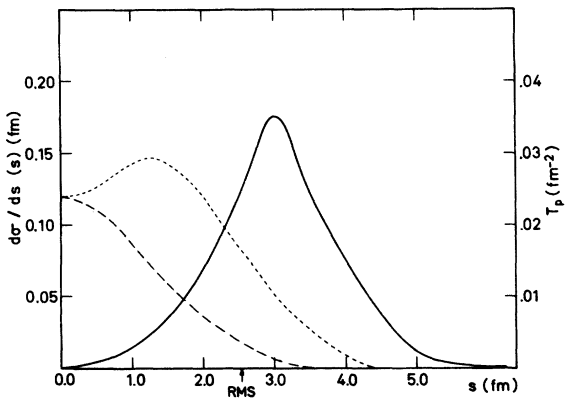

FIG. 1. The cross section $d\sigma/ds$ for the abrasion of one nucleon as a function of its distance from the center of the projectile (solid line). The dotted line (dashed line) shows the thickness function (which is a measure of the matter distribution) for p-wave nucleons (s-wave nucleons). Note how the abrasion cross section peaks at the surface outside the rms radius.

mentum distribution in the Wigner transformation Eq. (3.1). We use this relation to test various nuclear models. In order to have a fair comparison, i.e., to concentrate on their different predictions on the *surface* we impose the following two global conditions:

(i) All models for $W(\vec{R},\vec{k})$ reproduce the experimental density $\rho(\vec{R})$

$$\rho(\vec{R}) = \int d^3k\, W(\vec{R},\vec{k}). \tag{3.7}$$

(ii) All expressions for $W(\vec{R},\vec{p})$ have the same *global* mean square momentum

$$\langle \vec{k}^2 \rangle = \int d^3R\, d^3k\, \vec{k}^2 W(\vec{R},\vec{k}) \Big/ \int d^3R\, d^3k\, W(\vec{R},\vec{k}). \tag{3.8}$$

A value $\langle \vec{k}^2 \rangle^{1/2} = 174$ MeV/c is extrapolated from (e,e') experiments Ref. 1.

We consider four models. The *uniform Fermi gas* model (UFG) for the nucleus has the Wigner transformation

$$W_{\mathrm{UFG}}(\vec{R},\vec{k}) = \rho(\vec{R}) \frac{3}{4\pi p_F{}^3}\, \Theta(p_F{}^2 - \vec{k}^2). \tag{3.9}$$

Spatial density $\rho(\vec{R})$ and momentum distribution are decoupled; nucleons move everywhere with the same momenta.

The *local Fermi gas* model (LFG) retains the simple form of Eq. (3.9),

$$W_{\mathrm{LFG}}(\vec{R},\vec{k}) = \rho(\vec{R}) \frac{3}{4\pi p_F{}^3(R)}\, \Theta[p_F{}^2(R) - k^2], \tag{3.10}$$

but $p_F(R)$ is the local Fermi momentum

$$p_F(R) = p_F(0)[\rho(\vec{R})/\rho(0)]^{1/3}. \tag{3.11}$$

The constant $p_F(0)$ is adjusted according to the requirement Eq. (3.8). In the LFG model, nucleons move slower on the surface. For the *shell model* with harmonic oscillator functions (SM-HO) the Wigner transform can be given analytically

$$W_{\mathrm{SM-HO}}(\vec{R},\vec{k}) = \frac{2}{3\pi^2} e^{-R^2/b^2} e^{-k^2 \cdot b^2} \left(\frac{R^2}{b^2} + k^2 b^2 - 1 \right) \tag{3.12}$$

with the oscillator parameter $b = 1.75$ fm for ^{16}O. Finally, the *shell model* with *Hartree-Fock* wave functions (SM-HF) leads to a Wigner transform

$$W_{\mathrm{SM-HF}}(\vec{R},\vec{k}) = \int \frac{d^3r}{(2\pi)^3} e^{-i\vec{k}\cdot\vec{r}} \times \sum_\beta \Psi_\beta^*\left(\vec{R} - \frac{\vec{r}}{2}\right) \Psi_\beta\left(\vec{R} + \frac{\vec{r}}{2}\right). \tag{3.13}$$

If the numerical single particle wave functions Ψ_β are expanded in a harmonic oscillator basis, the Wigner transform can be calculated using Moshinsky's transformation brackets (Appendix C). In our calculation the wave functions Ψ_β have been obtained from a calculation by Campi.[16]

The experimental data are used in two ways to test nuclear models: We compare calculated and experimental *widths* for all four models and look at the *shapes* of the momentum distributions only for the shell model distributions. Table I shows the comparison of experimental and calculated widths.

$$\langle k_\parallel{}^2 - \langle k_\parallel \rangle^2 \rangle_{k_\perp = 0} = \int_{\langle k_\parallel \rangle}^{\infty} dk_\parallel\, k_\parallel{}^2 \frac{d^3\sigma}{dk^3}\Big|_{\vec{k}_\perp = 0} \times \left(\int_{\langle k_\parallel \rangle}^{\infty} dk_\parallel \frac{d^3\sigma}{dk^3}\Big|_{\vec{k}_\perp = 0} \right)^{-1}. \tag{3.14}$$

Note the requirement $k_\perp = 0$. An average without this constraint,

$$\langle k_\parallel{}^2 - \langle k_\parallel \rangle^2 \rangle = \int d^3k\, k_\parallel{}^2 \frac{d^3\sigma}{dk^3} \times \left(\int d^3k \frac{d^3\sigma}{dk^3} \right)^{-1}, \tag{3.15}$$

gives a different width. The experimental value in Table I has been recalculated from the data (for $k_\parallel > \langle k_\parallel \rangle$) and is smaller (by 10 MeV/c) than the value obtained from a Gaussian fit.[3] This difference is explained by the fact that the experi-

TABLE I. The widths of the experimental and calculated cross sections for the fragmentation reaction $^{16}O+^{12}C \rightarrow ^{15}O+X$.

Nuclear model	$\langle k_\parallel^2\rangle^{1/2}_{k_\perp=0}$ [MeV/c]
uniform Fermi gas	130
local Fermi gas	33
Shell model (harmonic oscillator)	91
Shell model (Hartree-Fock)	86
Experiment	89

mental distribution is *not* a pure Gaussian (Fig. 2).

According to the table, the uniform Fermi gas predicts too large a momentum on the surface while the local Fermi gas predicts too small momenta. The two shell models do well for the width. In order to test them more severely, we calculate the *shapes* of the cross section from the two models and compare them with experiment (Fig. 2). Both models work well for momenta below and around $p_F = 225$ MeV/c, but the harmonic oscillator model falls off much too rapidly for large momenta. As expected, the Hartree-Fock functions do much better. The wave functions of Ref. 16 are given in a harmonic oscillator basis which is truncated at the $8p$ orbit. We suspect that the remaining discrepancy at the high momentum end is due to the insufficiency of these eight terms in reproducing the actual wave function. But on the whole, the agreement is gratifying.

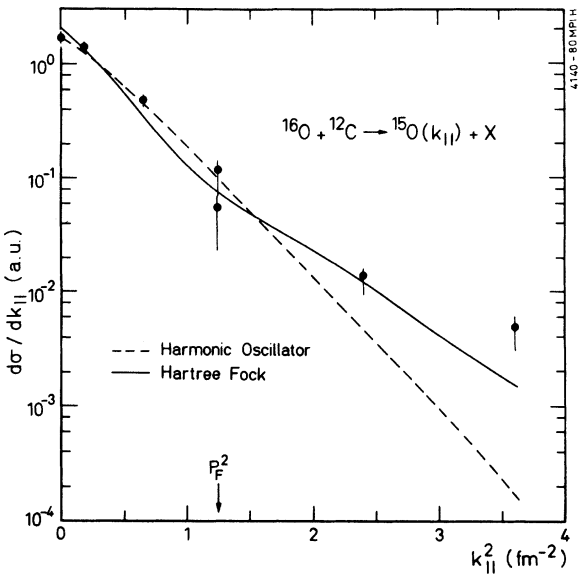

FIG. 2. The momentum distribution of ^{15}O fragments (arbitrary units) in the projectile's frame as a function of $k_\parallel^2$. Displayed are calculations with two models: the shell model (harmonic oscillator) and the shell model (Hartree-Fock), as well as the experimental data. The curves have been normalized relative to each other in order to have the same area $\int dk_\parallel d\sigma/dk_\parallel$.

IV. AN IDEAL EXPERIMENT

In this paper we have related the cross section $d^3\sigma/dk^3$ for a fragmentation reaction to the momentum distribution of the removed nucleon on the surface. The relation has been successfully tested with a particular experiment. Thus we think that experiments of this type may be a useful and reliable tool to measure momentum distributions in nuclei. High energy reactions can thus be used to investigate nuclear structure. The derivation and discussion in the previous chapters can be summarized in the following recommendations for an ideal experiment: If $\vec{k}$ denotes the momentum of the fragment in the projectile's rest frame, the quantity

$$\frac{d\sigma}{dk_\parallel} = \int d^2k_\perp \frac{d^3\sigma}{dk^3}, \quad k_\parallel > \langle k_\parallel\rangle. \tag{4.1}$$

is most useful. That is, the cross section for a particular $k_\parallel$ should be integrated over all transverse components. In this way many theoretical approximations are not necessary and a direct relation to the nuclear momentum distribution [Eq. (1.3)] is obtained. The energy of the incident projectile should be "sufficiently high" for two reasons: The Glauber theory, which underlies the derivation of Eq. (1.3), works better the higher the energy, and a lower limit may be 500 MeV/nucleon. At this energy the kinematical limit is $k_\parallel^{\max} = 410$ MeV/c and therefore the neglect of energy conservation might be dangerous. Projectile energies of 1 GeV/nucleon and 2 GeV/nucleon have kinematical limits of 530 MeV/c and 640 MeV/c, respectively, and permit us to measure a wider range of intrinsic momenta.

The experiment should concentrate on values $k_\parallel > \langle k_\parallel\rangle$, since for negative $k_\parallel$ multiple scattering effects, which have no relation to intrinsic momentum distributions, degrade the spectrum. The experiment should be performed with light targets in order to reduce the Coulomb breakup.[15] The momenta of those fragments are not related to intrinsic momenta. Protons as targets would be very useful. In this case the coherent breakup cross section would be zero.

Experiments with the removal of more than one nucleon have been performed, such as

$$^{16}O + \text{target} \rightarrow ^{14}N + X. \tag{4.2}$$

What can be learned from the momentum distribution of ^{14}N? Unfortunately, it is not easily related to the momentum distribution of two nucleons in ^{16}O. The reason is the reaction dynamics[15]: A ^{14}N nucleus can be formed in two ways from reaction (4.2):

(i) Two nucleons can be removed directly in a high energy process with the ^{14}N remaining in a bound state. This process measures properties of a nucleon pair in ^{16}O.

(ii) One nucleon is removed from ^{16}O in a fast process, at the same time the intermediate nuclei ^{15}O or ^{15}N are excited and later decay into ^{14}N. In this case the momenta of ^{14}N measure the single-nucleon distribution in ^{16}O modified by the distribution of a recoil nucleon in the decay.

The relative importance of (i) to (ii) is about 2 to 1 for reaction (4.2).[15]

The origin of the momentum distribution of nucleons in nuclei is twofold: The average shell model potential together with the Pauli principle lead to a smooth momentum distribution characterized by the Fermi momentum. High momentum components in nuclei are attributed to nucleon-nucleon correlations. The fragmentation experiment measures the shell model part for the following reason: The requirement that the fragment remains in a bound state limits the state of the removed nucleon prior to the collision to a shell model orbit.

ACKNOWLEDGMENTS

We have enjoyed the help of many colleagues. Professor M. Simbel helped us find an error in the calculation. Professor X. Campi provided the results of a Hartree-Fock calculation. Doctor H. C. Chiang, Dr. T. Fujita, Dr. F. Hachenberg, Dr. A. Klar, Dr. H. Krimm, Dr. H. J. Pirner, and Prof. T. H. Seligman helped us to clarify the physics. This work was supported in part by a grant from the Federal Ministry for Research and Technology (BMFT).

APPENDIX A

In order to estimate the total coherent fragmentation cross section

$$\sigma^{\mathrm{coh}}=\int d^3k \int d^3q \sum_{\alpha}{}' |a_\alpha|^2 \left| \int \frac{d^2b}{2\pi} e^{-i\vec{q}\cdot\vec{b}} e^{i\chi_{FT}(\vec{b})} \int d^3x\, \eta^*_{\vec{q}-\vec{k}}(\vec{x}) e^{i\chi_T(\vec{b}+\vec{x})} \varphi_\alpha(\vec{x}) \right|^2, \tag{A1}$$

we make two approximations. The functions $e^{i\chi_{FT}(\vec{b})}$ and $e^{i\chi_T(\vec{b}+\vec{x})}$ will give their maximum contributions at $b^2 \approx (R_T+R_P)^2$ and $(\vec{b}+\vec{x})^2 \approx R_T{}^2$, respectively. Therefore, one expects an expansion around $\vec{x}=-\vec{b}R_T/(R_T+R_P)$ to converge rapidly and write

$$\chi_T(\vec{b}+\vec{x}) \simeq \chi_T\left(\vec{b}\,\frac{R_P}{R_P+R_T}\right) + \left(\vec{x}+\frac{\vec{b}R_T}{R_P+R_T}\right)\nabla\chi_T\left(\vec{b}\,\frac{R_P}{R_P+R_T}\right). \tag{A2}$$

Inserting (A2) into (A1),

$$\sigma^{\mathrm{coh}}=\int d^3k \int d^2q \sum_{\alpha}{}' |a_\alpha|^2 \left| \int \frac{d^2b}{2\pi} e^{-i\vec{q}\cdot\vec{b}} \exp\left[i\chi_{TF}(\vec{b}) + i\chi_T\left(\vec{b}\,\frac{R_T}{R_T+R_P}\right)\right] \int d^3x\, \eta^*_{\vec{k}-\vec{q}}(\vec{x})\vec{x}\cdot\nabla\chi_T\varphi_\alpha(\vec{x}) \right|^2. \tag{A3}$$

The momentum $\vec{\nabla}\chi_T$ is estimated from the knowledge of the optical potential to be of the order of 40 MeV/c. This small value ensures rapid convergence of (A2) and permits the truncation in (A3). Since for ^{16}O as the projectile the bound state φ is a $1p$ orbit (well approximated by a harmonic oscillator wave), the operator $\vec{x}$ only connects to the $1d$ orbit or the $1s$ orbit, the latter being forbidden by the Pauli principle. Therefore we exhaust the integral over final states by the $1d$ orbit and find

$$\sigma^{\mathrm{coh}} \leq 4 \text{ mb}. \tag{A4}$$

APPENDIX B

The wave function $\eta_{\vec{q}-\vec{k}}$, Eq. (2.2), of the neutron which is removed from the projectile is a plane wave modified by the final state interaction with the fragment nucleus. In a coherent fragmentation event, the neutron receives small recoil momentum and the orthogonality Eq. (2.5) is the most important consequence of the final state interaction. In an incoherent fragmentation process (a hard collision) the nucleon receives a mainly transverse recoil momentum which is fairly large (400 MeV/c). Then the nucleon reacts in two

ways with the fragment.

(i) The struck nucleon recoils *into* the fragment, deposits all or part of its recoil energy (of order 100 MeV). The fragment will be excited to a particle unstable state and decay by emitting more nucleons.[15,18] Those nuclei are not observed. Hence the final state interaction reduces the cross section of reaction (1.1).

(ii) The removed nucleon is bound in a shell-model potential before the interaction. The motion out of the potential leads classically to a small observable shift $\langle k_{\parallel}\rangle$ in the experimental momentum distribution. This is quantitatively understood.[19] The detailed calculation of Ref. 6 with a distorted wave η, calculated from a separable potential, does not show significant changes in the longitudinal spectrum (in the transverse direction the modifications are significant).

APPENDIX C

An analytical expression for the Wigner function, calculated from a general one-body density matrix $\langle\vec{r}|\rho|\vec{r}'\rangle$, can be derived, provided $\langle\vec{r}|\rho|\vec{r}'\rangle$ is given in the form

$$\langle\vec{r}|\rho|\vec{r}'\rangle=\sum_{\substack{n_1l_1m_1\\n_2l_2m_2}} a_{n_1l_1m_1}a^*_{n_2l_2m_2}\Psi_{n_1l_1m_1}(\vec{r})\Psi^*_{n_2l_2m_2}(\vec{r}')\,, \tag{C1}$$

where Ψ_{nlm} are harmonic oscillator wave functions and a_{nlm} are arbitrary expansion coefficients. The corresponding Wigner function is defined

$$W(\vec{R},\vec{p})=\sum_{\substack{n_1l_1m_1\\n_2l_2m_2}} a_{n_1l_1m_1}a^*_{n_2l_2m_2}W^{n_2l_2m_2}_{n_1l_1m_1}(\vec{R},\vec{p})\,, \tag{C2}$$

where

$$W^{n_2l_2m_2}_{n_1l_1m_1}(\vec{R},\vec{p})=\frac{1}{(2\pi)^3}\int d^3y e^{-i\vec{p}\cdot\vec{y}}\Psi^*_{n_2l_2m_2}\left(\vec{R}-\frac{\vec{y}}{2}\right)\Psi_{n_1l_1m_1}\left(\vec{R}+\frac{\vec{y}}{2}\right). \tag{C3}$$

The idea is to consider instead

$$W^{n_1l_1\lambda\mu}_{n_2l_2}(\vec{R},\vec{p})=\int\frac{d^3y}{(2\pi)^3}e^{-i\vec{p}\cdot\vec{y}}\sum_{m_1m_2}\langle\lambda\mu\,|\,l_1m_1l_2-m_2\rangle\Psi_{n_1l_1m_1}\left(\vec{R}-\frac{\vec{y}}{2}\right)\Psi_{n_2l_2-m_2}\left(\vec{R}+\frac{\vec{y}}{2}\right), \tag{C4}$$

which couples the angular momentum of the two particles to a total angular momentum λ with projection μ. $\langle\lambda\mu\,|\,l_1m_1l_2-m_2\rangle$ is the corresponding Clebsh-Gordan coefficient.

Now we introduce the variable transformation $(\vec{R},\vec{y},\vec{p})\to(\vec{R}',\vec{y}',\vec{p}')$

$$\begin{aligned}\vec{R}'-\vec{y}'&=\sqrt{2}\left(\vec{R}-\frac{\vec{y}}{2}\right),\\ \vec{R}'+\vec{y}'&=\sqrt{2}\left(\vec{R}+\frac{\vec{y}}{2}\right),\\ \vec{p}'&=\sqrt{2}\,\vec{p}\,.\end{aligned} \tag{C5}$$

Then (C4) can be rewritten as

$$W^{n_1l_1\lambda\mu}_{n_2l_2}(\vec{R}',\vec{p}')=\int\frac{d^3y'}{(2\pi)^3}2^{3/2}e^{i\vec{p}'\cdot\vec{y}'}\sum_{m_1m_2}\langle\lambda\mu\,|\,l_1m_1l_2-m_2\rangle\Psi_{n_1l_1m_1}\left[\frac{1}{\sqrt{2}}(\vec{R}'-\vec{y}')\right]\Psi_{n_2l_2-m_2}\left[\frac{1}{\sqrt{2}}(\vec{R}'+\vec{y}')\right]. \tag{C6}$$

Using the Moshinsky transformation brackets,[20] the $\vec{R}'$ and $\vec{y}'$ dependence can now be decoupled, and the Fourier transform on $\vec{y}'$ can be explicitly evaluated

$$W^{n_1l_1\lambda\mu}_{n_2l_2}(\vec{R}',\vec{p}')=2^{3/2}\sum_{\substack{NLnl\\m\mathcal{M}}}\langle NLnl\lambda\,|\,n_1l_1n_2l_2\lambda\rangle\langle\lambda\mu\,|\,LMlm\rangle\Psi_{NL\mathcal{M}}(\vec{R}')\tilde{\Psi}_{nlm}(\vec{p}')\,. \tag{C7}$$

$\tilde{\Psi}_{nlm}$ is the Fourier transform of the harmonic oscillator wave function

$$\tilde{\Psi}(\vec{p}) = \int \frac{d^3y}{(2\pi)^3} e^{-i\vec{p}\vec{y}} \Psi(\vec{y}) , \tag{C8}$$

and $\langle NLnl\lambda \,|\, n_1 l_1 n_2 \lambda\rangle$ are the Moshinsky transformation brackets as defined in Ref. 20.

Now by using the orthogonality of Clebsh-Gordan coefficients, one can evaluate (C3)

$$W^{n_1 l_1 m_1}_{n_2 l_2 m_2}(\vec{R}', \vec{p}') = (-)^{m_2} \sum_{\substack{NLnl \\ m M \lambda}} \langle \lambda m_1 - m_2 \,|\, l_1 m_1 l_2 - m_2\rangle \langle \lambda \mu \,|\, m L l m\rangle \langle NLnl\lambda \,|\, n_1 l_1 n_2 l_2 \lambda\rangle \Psi_{NLM}(\vec{R}') \tilde{\Psi}_{nlm}(\vec{p}') . \tag{C9}$$

To obtain the Wigner function W one has now only to construct the linear superposition of the $W^{n_2 l_2 m_2}_{n_1 l_1 m_1}$ according to (C2).

---

[1] E. J. Moniz, I. Sick, R. R. Whitney, J. R. Ficenec, R. D. Kephart, and W. P. Trower, Phys. Rev. Lett. 26, 445 (1971).

[2] J. Mougey, M. Bernheim, A. Bussière, A. Gillebert, Phan Xuan Hô, M. Priou, D. Royer, I. Sick, and G. J. Wagner, Nucl. Phys. A262, 461 (1976).

[3] D. E. Greiner, P. J. Lindström, H. H. Heckman, B. Cork, and F. S. Bieser, Phys. Rev. Lett. 35, 152 (1975), and private communication.

[4] A. S. Goldhaber, Phys. Lett. 53B, 306 (1974).

[5] A. Y. Abul-Magd and J. Hüfner, Z. Phys. A 227, 379 (1976).

[6] T. Fujita and J. Hüfner, Nucl. Phys. A343, 493 (1980).

[7] R. Shyam, G. Baur, F. Rösel, and D. Trautmann, Phys. Rev. C 19, 1246 (1979).

[8] R. Glauber, Phys. Rev. 99, 1515 (1955).

[9] A. I. Akhieser and A. G. Sitenko, Phys. Rev. 106, 1236 (1957).

[10] L. Bertocchi and A. Tékou, Nuovo Cimento 21A, 223 (1974); L. Bertocchi and D. Treleani, *ibid.* 36A, 1 (1976).

[11] J. H. Kühn and S. A. Nissen-Meyer, Nucl. Phys. A312, 409 (1978).

[12] R. J. Glauber, in *Lectures in Theoretical Physics*, edited by W. E. Brittin and L. G. Dunham (Interscience, New York, 1959), Vol. I.

[13] R. J. Glauber and G. Matthiae, Nucl. Phys. B21, 135 (1970).

[14] H. H. Heckman and P. J. Lindstrom, Phys. Rev. Lett. 37, 56 (1976).

[15] P. J. Lindstrom, D. E. Greiner, H. H. Heckman, B. Cork, and F. S. Bieser, Lawrence Berkeley Laboratory Report No. LBL-3650 (unpublished).

[16] X. Campi, private communication.

[17] A. Y. Abul-Magd and J. Hüfner, Nucl. Phys. A308, 429 (1978).

[18] J. Hüfner, K. Schäfer, and B. Schürmann, Phys. Rev. C 12, 1888 (1975).

[19] A. Y. Abul-Magd, J. Hüfner, and B. Schürmann, Phys. Lett. 60B, 327 (1976).

[20] T. A. Brody and M. Moshinsky, *Tables of Transformation Brackets* (Gordon and Breach, New York, 1967).